
Vibrational and Thermal Measurements of Laser Guide Star Adaptive Optics for Tracking Space Debris

Research School of Astronomy and Astrophysics
ANU College of Physical and Mathematical Sciences
The Australian National University

Abstract

Accurately tracking space debris can reduce the possibility of orbital collisions. Performance of Laser Guide Star Adaptive Optics (LGS AO)- assisted laser tracking stations are dependent upon telescope and LGS AO components. The guidestar laser vibration environment and Coudé mirror temperature gradients were measured to improve performance of Mount Stromlo laser-tracking station.

Revision History

Version No.	Author	Date	Description	Verification
0.1	A. Stuchbery & E. Thorn,	December 1, 2014	Draft	
0.2	A. Stuchbery & E. Thorn,	December 2, 2014	Draft with corrections	
0.3	A. Stuchbery & E. Thorn,	December 10, 2014	Draft inc methodology and Lit Review	
0.4	A. Stuchbery & E. Thorn,	January 6, 2015	Draft - experimentation started	
0.5	A. Stuchbery & E. Thorn,	January 9, 2015	experimentation complete	
0.6	A. Stuchbery & E. Thorn,	January 23, 2015	Vib. analysis draft complete	
1.0	A. Stuchbery & E. Thorn,	January 30, 2015	Complete Report	

Contents

1	Introduction	4
1.1	Document Purpose	4
1.2	Document Scope	4
1.3	Intended Audience	4
1.4	Acronyms and Abbreviations	4
1.5	Definitions	4
2	Project Definition	5
2.1	Background	5
2.2	Objective	5
2.3	Scope	5
2.4	Approach	5
2.5	Stakeholders	6
2.6	Deliverables and Outcomes	6
3	Project and Engineering Management	7
3.1	Project Organisation	7
3.2	Work Breakdown Structure and Schedule	7
3.3	Resourcing	10
3.4	Risk and Issue Management	11
4	Literature Review	11
4.1	Space Debris	11
4.2	Adaptive Optics	11
4.2.1	Sodium Guide Star Laser	12
4.2.2	Vibrations	12
4.3	Unknown Knowledge	13
5	Experiments and Methodology	13
5.1	Equipment List	13
5.2	Calibration and Testing	13
5.3	Vibrational Experiment on Laser	14
5.4	Vibrational Experiment on Telescope	15
5.5	Thermal Experiment on Coude Mirrors	17
6	Results and Discussion	19
6.1	Laser Unit Vibrations	19
6.2	Telescope Dome	21
6.2.1	Mechanical Operations	21
6.2.2	Instrumentation	24
6.2.3	Acoustic Vibration	24
6.3	Thermal Measurements	24
6.3.1	Maximum and Minimum Temperature Components	24
6.3.2	Lag Times	26
6.3.3	Decay Curves	28
7	Conclusions and Recommendations	30
8	Future Work	31

9 Appendix	32
------------	----

List of Figures

1 Project Organisation	7
2 Work Breakdown Structure	8
3 Project Schedule	9
4 Adaptive Optics	12
5 Thermal Calibration Curves	14
6 Laser optical lab setup	15
7 Vibration Setup	16
8 Thermal Sensor Locations	17
9 Location of Coude Mirrors 4 & 5	18
10 Laser Deterioration	20
11 Spectra of laser failure	21
12 Baseline spectrum in dome	22
13 Vibrations from telescope tracking	23
14 Recorded thermal data	25
15 Three day time-slice	26
16 Three day representative data.	27
17 Lag times	28
18 Data used for curve fitting.	29
19 Three day representative data.	30
20 Emissivity	31

List of Tables

1 Deliverables	6
2 Personnel Resources	10
3 Material Resources	10
4 EOS Personnel Resources	10
5 Risks and Issue Management	11
6 Laser bench tests	16
7 Telescope dome tests	17
8 Measurements	18
9 Laser bench results	19
10 Telescope dome tests	22
11 Telescope dome tests	24
12 Maximum/Minimum Temperatures per component	25
13 k values	29
14 Frequencies and Magnitudes	32

1 Introduction

1.1 Document Purpose

The objective of this project is to investigate and evaluate the vibrational modes and magnitudes that may potentially affect the operation of the Sodium Guide Star Laser (GSL) to be attached to the Mount Stromlo 1.8 metre telescope. Additionally, thermal measurements will be undertaken on the Coude mirrors and their mounts to be fed into a stability analysis by glseos Space Systems.

1.2 Document Scope

Project management plan and report for the vibrational and thermal analysis project using details and experiments completed as of January 30, 2015.

1.3 Intended Audience

- Electro Optic Systems (EOS) Space systems
- Australian National University (ANU)

1.4 Acronyms and Abbreviations

Acronyms

AITC Advanced Instrumentation and Technology Centre. 5, 10

ANU Australian National University. 4, 6, 11

AO Adaptive Optics. 4, 11, 12

EOS Electro Optic Systems. 4, 6, 10, 11, 13

GSL Guide Star Laser. 4, 5, 10, 12, 13, 14, 16, 18, 22, 23, 30, 31

LGS Laser Guide Star. 4

RTDs Resistance Thermometer Detectors. 17

1.5 Definitions

- Adaptive Optics (AO): First conceived in 1959 by Horace Babcock, Adaptive Optics (AO) is the process of using deformable mirrors and wavefront sensors in closed feedback loops to account for distortions caused by atmospheric turbulence [1, 2].
- Laser Guide Star (LGS): A Laser Guide Star (LGS) is an artificial star or light source generated in the atmosphere to allow for AO operation without the presence of a natural guide star or bright enough reference source [3–5].
- Guide Star Laser (GSL): A GSL is a laser used to create a LGS [3, 4].
- Mechanical Vibrations: A periodic process of oscillation with respect to an equilibrium point.
- Acoustic Vibrations: Vibrations induced due to acoustic pressure waves through air.

2 Project Definition

2.1 Background

The AO system to be used on the EOS and ANU 1.8 metre telescope requires installation of a sodium GSL in order to accurately track space debris. The AO GSL is currently under development within EOS optical labs and is highly sensitive to vibration. The vibrational characteristics of the location where the unit is to be housed within the 1.8 metre telescope dome are unknown. These characteristics need to be discovered in order that the GSL performs without issue. Also of interest are the Coude mirrors and their mounts. These mounts require frequent realignment otherwise telescope performance suffers. It is suspected that temperature changes in mount components may be affecting mirror alignment.

2.2 Objective

- Main Objectives
 - Determine the frequency range - spectrum - of the vibrational output of the telescope for use in the design of the GSL mount.
 - Identify peak and peak-to-peak values of mechanical oscillation induced by the telescope.
 - Measure the temperatures of the: outside ambient air, dome interior air, surface of the mirror mounts, and the surface of the Coude mirrors.
- Secondary Objectives (if time allows)
 - Identify the current working vibrational conditions of the GSL unit.

2.3 Scope

A comprehensive experimental vibrational analysis is to be conducted to evaluate the extent of mechanical oscillation that the telescope inputs into the GSL. This analysis will indicate whether or not a damping system needs to be considered for future design and installation. However, design considerations of a damping system are beyond the scope of this project. A thermal analysis to determine what effect outside ambient air temperature has upon the surface temperatures of the Coude mirrors and their mounts will be performed. The project will conclude on January 30th. There will be an ANU Summer Scholars intern and an Advanced Instrumentation and Technology Centre (AITC) intern working on this project.

2.4 Approach

- Learn to operate and calibrate accelerometers and thermal sensors.
- Determine types of analysis relevant to the problem that could be done.
- Determine points of interest for thermal and motion analysis.
- Determine modes and length of testing required to perform analysis (experimentation potentially required here).
- Perform measurements.
- Analyse data.

-
- Remeasure and reanalyse as necessary.
 - Write report.

2.5 Stakeholders

- EOS Space Systems
- ANU

2.6 Deliverables and Outcomes

Table 1: Deliverables and milestones with due dates.

Item	Due Date (dd/mm/yy)	Additional Notes
REVIEW: Project Plan	28/11/14	
Project Plan	28/11/14	
Experimental Methodology Plan	3/11/14	(draft for approval)
Literature Review	5/12/14	
REVIEW: Literature Review	5/12/14	
Sensor Calibration	10/12/14	
Sensor Mount Construction	15/12/14	
Temperature Sensor Mounting and Data Logging	19/12/14	
Recover Temperature Data	05/01/15	
REVIEW: Abstract	07/01/15	
Abstract	09/01/15	
REVIEW: Final Report	19/01/15	
Presentation	22/01/15	
Final Report	30/01/15	

3 Project and Engineering Management

3.1 Project Organisation

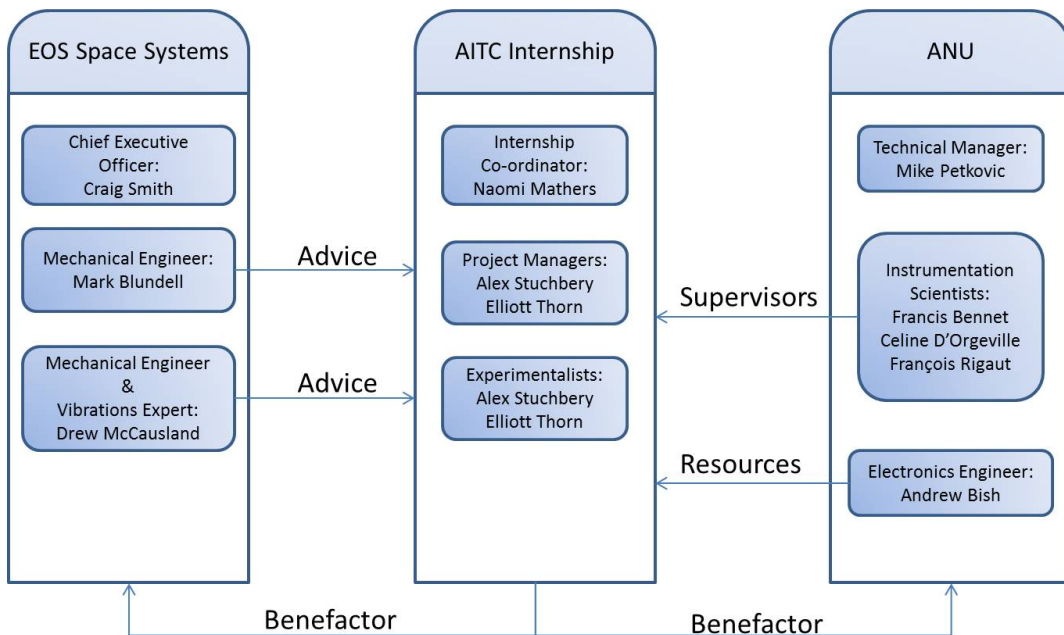


Figure 1: Diagram of project organisation of people, roles and governing organisations.

3.2 Work Breakdown Structure and Schedule

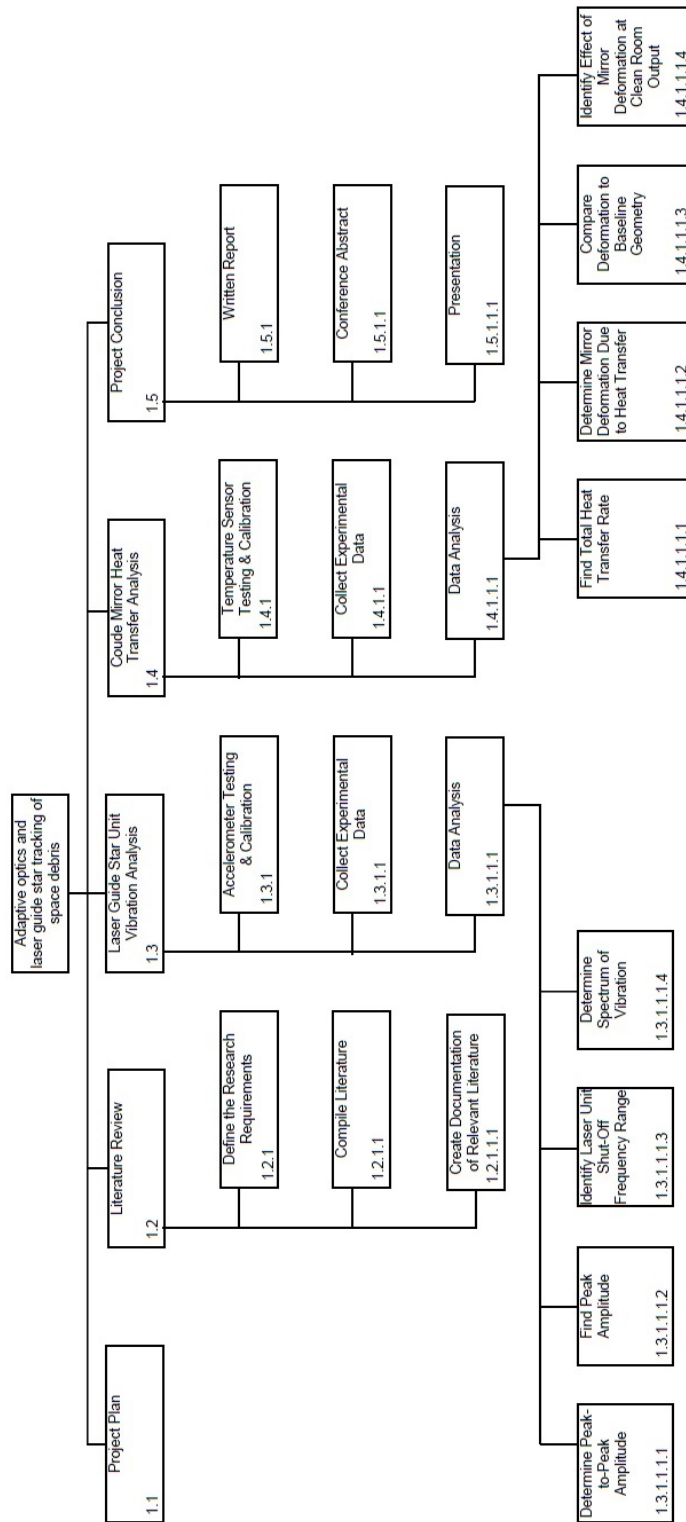


Figure 2: Work breakdown structure for the project.

Name	Predecessor	Completion	Start_Date	Finish_Date
Adaptive optics and laser guide star tracking				
Work Package 1: Sensor Collection and Calibration				
1.2.1: Define Research Requirements		✓	28/11/2014	3/12/2014
1.3.1: Accelerometer Calibration	1.2.1	✓	28/11/2014	10/12/2014
1.3.1: Accelerometer Mounting Construction	1.2.1	✓	3/12/2014	15/12/2014
1.4.1: Temperature Sensor Calibration	1.2.1	✓	28/11/2014	10/12/2014
1.4.1: Temperature Sensor Mounting Construction	1.2.1	✓	3/12/2014	15/12/2014
Work Package 2: Experimentation				
1.3.2: Collect Experimental Data (Vibrational)	1.3.1	✓	15/12/2014	
1.4.2: Collect Experimental Data (Thermal)	1.4.1	✓	15/12/2014	
Work Package 3: Analysis				
1.3.3: Data Analysis (Vibrational)	1.3.2	✓	13/01/2015	
1.4.3: Data Analysis (Thermal)	1.4.2	✓	13/01/2015	
Work Package 4: Write Report				
1.1: Project Management Report		✓	26/11/2014	28/11/2014
1.2: Literature Review		✓	28/11/2014	5/12/2014
1.1.1: Methodology and Experiments				
1.1.1: Results and Discussion	WP1 All Activities	✓		
1.1.1: Conclusions, Future Work and Executive Summary	WP3 All Activities	✓		
Work Package 5: Abstract	WP3 All Activities	✓		
1.1.2: Conference Abstract	WP 3 (Ideally WP 4)	✓		9/01/2015
Work Package 6: Presentation				
1.1.3: Presentation	WP 3	✓		22/01/2015

Figure 3: Schedule for the development of the program.

3.3 Resourcing

Distribution of personnel days to accomplish specific project deliverables have been assigned to A. Stuchbery and E. Thorn, Table 2.

Table 2: AITC personnel days allocated to specific work areas.

ID	Work Area	A. Stuchbery	E. Thorn	Allocated Days
1.1	Project Plan	2	2	4
1.2	Literature Review	3	3	6
1.3	GSL input vibration analysis	15	15	30
1.4	Coude mirror heat transfer analysis	12	12	24
1.5	Project conclusion	3	3	6
	Total	35	35	70

Material resources requisitioned to deliver project milestones are allocated, Table 3.

Table 3: Material resources allocated to work area ID codes.

ID	Item	Assignee	Item Details
1.3	piezoelectric accelerometer units	Project	Received from AITC
1.3	1.8 meter telescope	Project	Scheduled with EOS
1.3	Vibration analysis software	Project	Received from AITC
1.4	Assorted temperature sensors	Project	Received from AITC
1.4	1.8 meter telescope	Project	Scheduled with EOS
1.4	Heat transfer analysis	Project	Scheduled with EOS

EOS engineering consultative time requested, Table 4.

Table 4: EOS personnel hours allocated to specific work areas.

ID	Work Area	Mark Blundell	Drew McCausland	Telescope Control Tech.	Induction Coordinator	Allocated Hours
1.3	GSL vibration analysis	3	2	2	0.5	6.5
1.4	Coude mirror heat transfer analysis	2	-	1	-	4
	Total	5	2	3	0.5	10.5

3.4 Risk and Issue Management

Table 5: Potential risks and issues with plans for mitigation and relative likelihood.

Risk / Issue	Mitigation Strategy	Likelihood
Accelerometers not sensitive enough	Order more before Christmas	Moderate
Access to D. McCausland too limited	Get email and phone contacts	High
Thermal sensor failure over break	Setup sensors and test well before break to be sure they are working	Moderate

4 Literature Review

4.1 Space Debris

Over the last 40 years the problem of orbital space debris has become increasingly apparent [3, 4, 6–11]. The term space debris refers to all artificial objects which are in orbit and no longer operational [6]. The debris originate from objects such as decommissioned satellites, spent rocket stages and fragments from explosions in orbit [6, 7]. However the problem is not simply from this debris but from the propagation of this debris into a much larger cloud of smaller fragments via debris on debris collisions. As identified by Kessler and Cour-Palais [7] the fragments in orbit follow the same process as that of an asteroid belt on a much smaller time scale. This, if left untreated, could make certain regions of space impractical to enter without the expectation of damage from debris collisions [7]. At present there are tens of thousands of space debris objects over 10 cm in diameter with a combined mass of over 5 million kg [11] being tracked using RADAR tracking [12], and millions of fragments that are too small for us to track. The limitations on the accuracy of RADAR tracking from the large wavelengths used (2 m - 6 m) [4] have been identified as the primary cause for orbital collisions with high value satellites [8]. There are multiple strategies being considered to prevent further growth of the space debris from new launches such as - tethering, where spent rocket stages are connected to the main body via cables, active clean up spacecraft with missions dedicated to collecting and removing debris, and boosting satellites to a ‘graveyard’ orbit before decommissioning where no satellites are in operation [4]. However, there is no current solution to the problem of debris on debris collisions spreading debris into multiple smaller pieces which are much harder to track [10, 13]. A new technology that is being developed to solve this problem is laser tracking with AO to compensate for atmospheric turbulence [3, 4, 8, 14]. A specific example of this system being implemented is the ANU / EOS Space Debris Tracking Adaptive Optics Demonstrator [3, 4, 14] on the 1.8 metre telescope owned by EOS Space Systems at Mt. Stromlo, Canberra. This particular project is aimed to identify objects less than 10 cm in diameter and objects up to 3000 km in distance [3, 4].

4.2 Adaptive Optics

Adaptive Optics (AO) was first conceived in 1959 by Horace Babcock and is the process of using deformable mirrors and wavefront sensors in closed feedback loops to correct for distortions caused by atmospheric turbulence [1, 2, 5]. Adaptive optical systems on telescopes can give the same quality of image in the infra-red range as the Hubble Space Telescope has in the optical range as demonstrated by the Gemini telescope. The basic operation of an AO system is shown in figure 4. As well as a target, AO requires a guide star to determine what correction is required on the

deformable mirror [1, 2, 5]. For tracking fast moving objects, like space debris, a natural guide star made up by a real star or the debris itself is not possible so a Laser Guide Star (LGS) must be used [3, 4, 8, 14, 15].

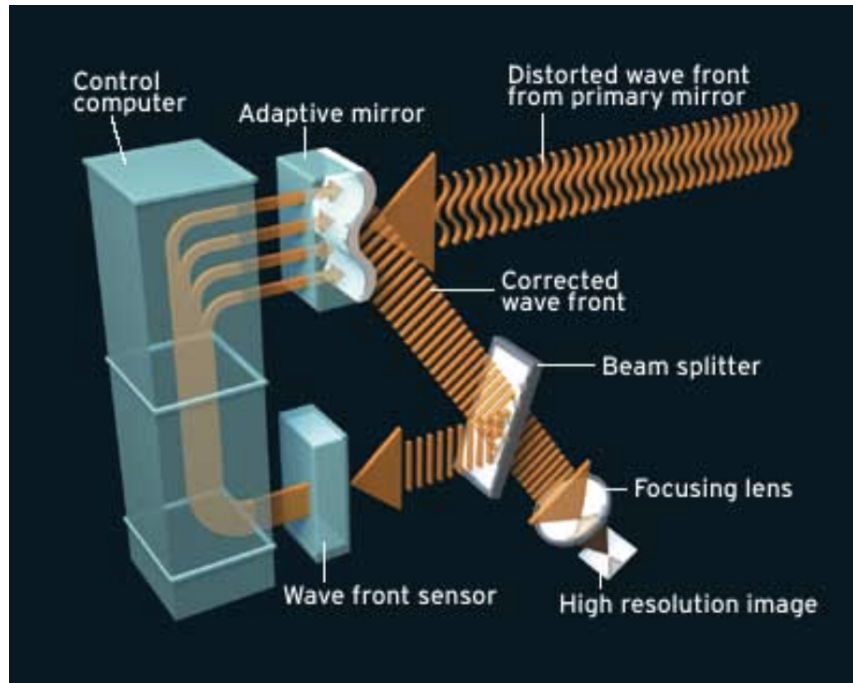


Figure 4: Diagram of the basic functioning of an adaptive optics system. Image from Lloyd-Hart [16].

4.2.1 Sodium Guide Star Laser

A sodium GSL is used to generate an artificial beacon at an altitude of approximately 90 km in the sodium layer of the atmosphere. A mechanism known as resonant backscattering is used to achieve this [17, 18]. Laser guide stars can be used when natural guide stars are not available or not bright enough [15, 19]. A GSL AO system is used in order, for instance, to sharpen astronomical images, enlarge sky coverage [19], or track smaller and more distant space debris [14]. The GSL demonstrator on the 1.8 m Mount Stromlo AO telescope utilizes a continuous wave 589 nm, 30 W average power output laser system [14] to excite sodium atoms in the mesosphere [20].

4.2.2 Vibrations

Vibration is defined as any motion that repeats after a time interval [21]. Vibration - with respect to telescope structures and instrumentation - may be caused by motors, cryocoolers, windshake, and fans [22]. This vibration becomes a problem for ground-based telescopes when it causes performance degradation [23]. In the case of Clenet et al. [24], a Strehl ratio degradation of up to 25% was attributed to mechanical vibration [24]. At the Gemini South facility a persistent vibration of 55 Hz was detected and found to be induced by the systems cryocooler - frequencies of 14 Hz and 100 Hz were also detected [25]. A major contributor to Strehl ratio loss at the EOS operated NACO telescope was vibration at 18 and 48 Hz, and the systems cryocooler was identified as a main source

of excitation [26]. Also viewed as sources of vibration were the telescope itself and its components i.e. the tip-tilt mechanism [27]. There are several approaches to reducing vibration excitation of ground-based telescopes however they are beyond the scope of this report. Based upon these examples it is expected that measurable vibration will be present between 0 and 100 Hz.

4.3 Unknown Knowledge

At present the vibrational characteristics of the 1.8 metre EOS telescope located at Mt. Stromlo, Canberra are unknown. The GSL being developed for mounting on the telescope is known to be sensitive to vibration. The vibrational environment of the telescope and laser construction laboratory need to be measured to factor into the laser and laser mount design. The exact levels of vibration required to cause reduction of performance and failure of the GSL are also unknown. Ideally this could be determined on both a whole-instrument and component level of the laser. A more easily achievable first step would be to determine the current vibrational working conditions of the laser, such that they could be compared to the vibrational conditions of the telescope.

5 Experiments and Methodology

5.1 Equipment List

- PCB J356B18 1000 mV/g accelerometer
- Sirius ACC
- Type 4294 Brue & Kjaer calibration exciter
- Appropriate accelerometer cabling
- Adhesive mounting wax
- 1 x 8 channel USB temperature logger Omega OM-USB-5203
- 4 x Ceramic platinum RTD Omega 1PT100KN1515CL1/10
- 2 x General purpose probes Omega ON-401-PP
- 2 x Attachable surface temperature probes Omega ON-409-PP
- Instacal software for sensor calibration and testing
- TracerDAQ software for interfacing temperature logger hardware with PC and data visualisation

5.2 Calibration and Testing

The accelerometers listed above were calibrated using a type 4294 Brue & Kjaer calibration exciter which is designed to deliver a constant 10 m s^{-2} vibration at 159.2 Hz. The calibration exciter was not calibrated itself to begin with but when the first accelerometer was tested it measured 9.99 m s^{-2} at 159.15 Hz. It is possible that the accelerometer or the exciter have drifted since their last calibration but it is unlikely that they have drifted by the exact same amount, hence the calibration exciter was deemed good enough to use as a basis for the calibration of all the accelerometers.

The temperature probes and RTDs were calibrated by submerging them into ice water and boiling water and logging the data over time. Ice water and boiling water are used in order to

determine known reference points for each probe - ice water at zero degrees and the boiling water temperature determined from the atmospheric pressure at the time of the test. Temperature vs time curves were produced from the logged data for each temperature probe figure 5.

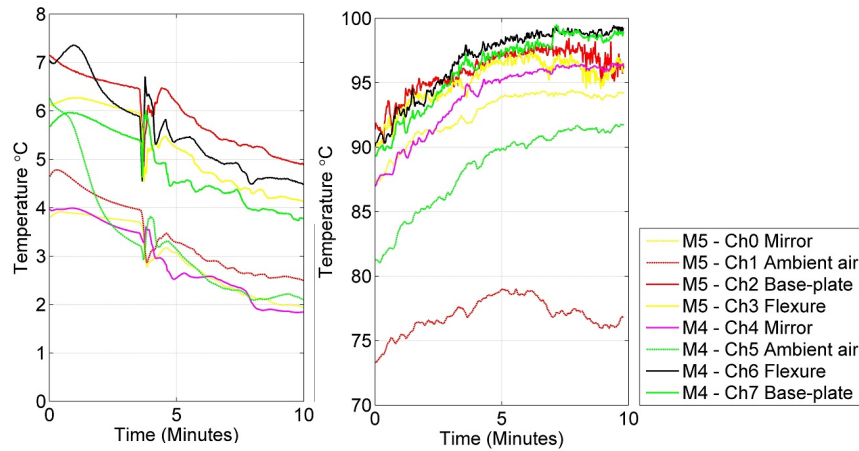


Figure 5: Left: ice-bath calibration curves. Right: boiling water calibration curves.

An average value over time was taken for each sensor to reduce noise at the known temperature points and that offset compensated for in the plotting of further data from the thermal sensors. Upon inspection of figure 5 right it appears that there may be a problem with the sensor recording data on channel 1. The channel 1 sensor appears to be reading approximately 6-7 °C lower than the sensor recording channel 5 - these sensors are of the same type. The data from this sensor should be treated with caution as it appears that it may be erroneous.

5.3 Vibrational Experiment on Laser

The PCB J356B18 3-axis 1000 mV/g accelerometer was mounted on the optical bench supporting the GSL with adhesive wax. Its orientation with respect to the optical bench (figure ??). The accelerometer was measuring at a frequency of 5000Hz which is well above the Nyquist-Shannon rate for the expected signals of interest; 0 - 100 Hz. The chillers labeled ‘a’, ‘b’ and ‘c’ are a Termotek p307-14176, a SMC Thermo-con HEC002-A5B-XA06006 and a Termotek P320-16744-1, respectively

The accelerometer’s x , y , and z -axes were connected to the Sirius unit’s channel 1, 2, and 3, respectively. Channel 7 received an output from the system’s piezo-actuator control unit measuring the degree to which the actuators were moving to compensate for vibrations. Channel 8 received an output from a photodiode measuring the light escaping from a resonant optical cavity in an undesirable direction - escaping light detected by the photodiode means less power in the final laser beam.

The tests performed are shown in Table 6. NOTE: Unless specified, the chillers are not running. When it is specified that a chiller has been turned on, no other chiller is active.

The Sirius unit heats up when in operation and automatically activates its cooling fans. During testing it was found that these cooling fans are detected by the accelerometer. For this reason the Sirius unit, and connected laptop, were placed on a table separate from the optical bench in order to minimise any vibration that it may induce in the measurements. The measurements were then analysed using the Dewesoft X software package.

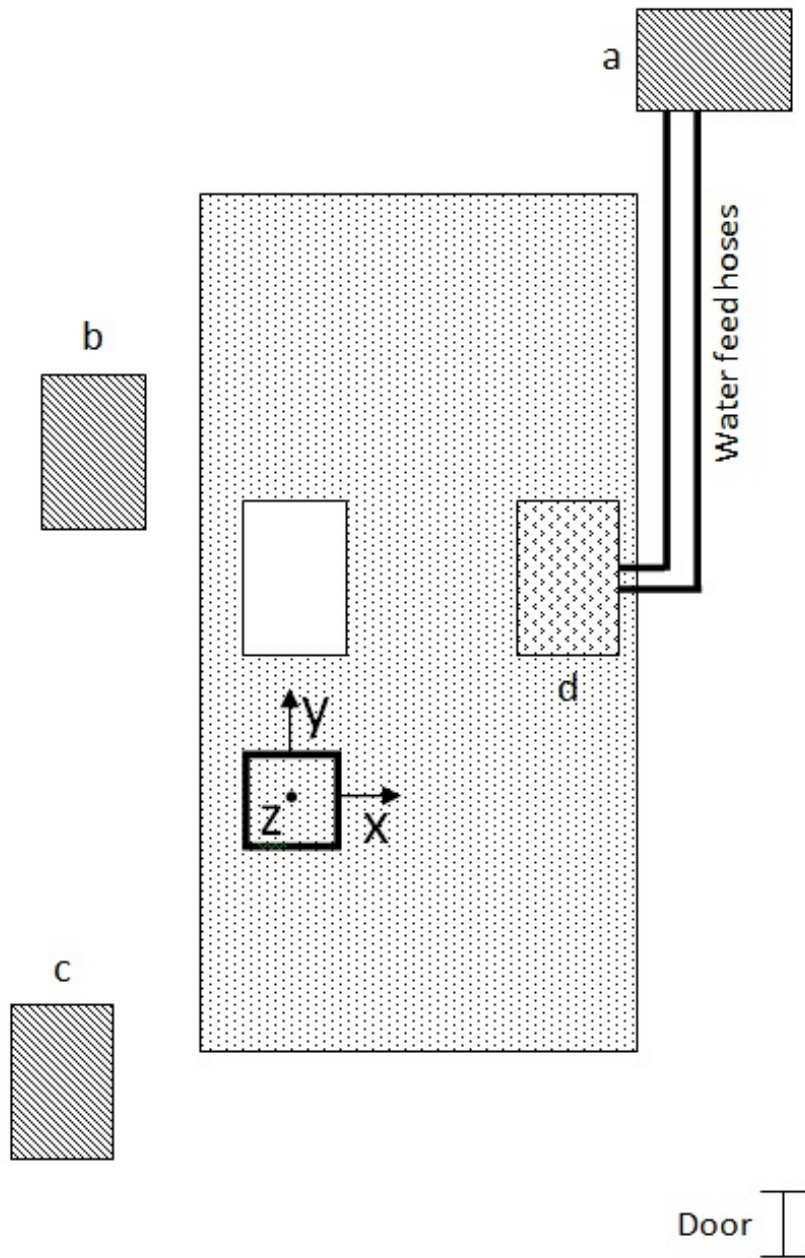


Figure 6: The accelerometer's x-axis points along the width of the bench, and the y-axis points along the length of the bench. The z-axis is pointed toward the ceiling. Also shown - represented as a white rectangle - is the optical setup. The blacked hashed rectangles, labeled 'a', 'b', and 'c', are the chillers. Note that chiller 'a' is connected via water hoses to a laser generation component labeled 'd'.

5.4 Vibrational Experiment on Telescope

The 1000 mV/g accelerometer was screwed into the telescope as shown in figure 7 using a M5 to M8 adapter. The cables were strain relieved using zip ties and kept away from moving parts. The

Table 6: Summary of tests performed on the laser containing optical bench.

Test number	Description
1	No activity.
2	Clapping along x-axis.
3	Clapping along y-axis.
4	Talking loudly.
5	Tapping bench by hand in negative z direction.
6	Slamming door to lab.
7	Chiller 'a' effect of switching on.
8	Chiller 'a' running.
9	Chiller 'a' running with water feed hoses removed.
10	Chiller 'b' running.
11	Chiller 'b' on effect on laser lock
12	Chiller 'b' on effect on laser lock 02
13	Chiller 'b' on and walking around bench.
14	Chiller 'c' running.

x, *y* and *z* axis are shown in figure 7 and were connected to channels 1, 2, and 3, respectively.

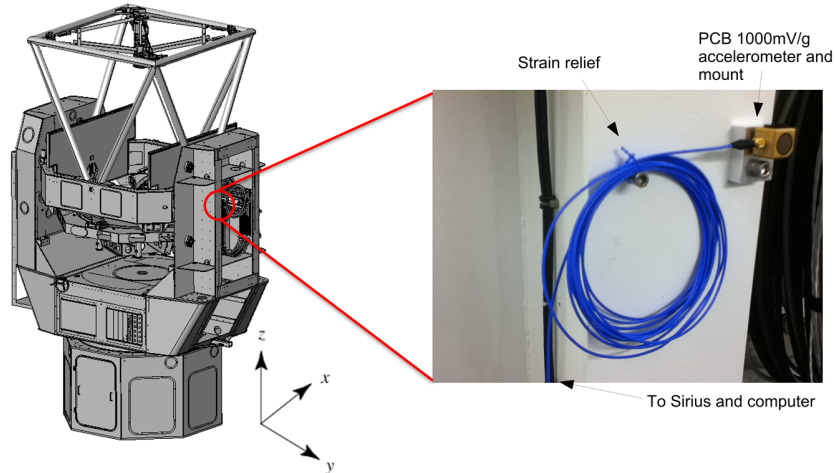


Figure 7: Diagram of the experimental setup used to measure the vibrations on the 1.8 metre telescope.

The telescope operations summarised below in Table 7 were performed and recorded. Analysis was then performed using the Dewesoft X software package.

Table 7: Summary of tests performed in the telescope dome.

Test number	Description
1	No activity.
2	Altitude motion up.
3	Altitude motion down.
4	Full azimuth rotation.
5	Tapping left side of GSL mount.
6	Tapping right side of GSL mount.
7	Tapping trunnion nasmyth.
8	Tapping truss mid head-ring.
9	Mirror covers opening.
10	Side dome shutters opening.
11	Middle camera operating.
12	Thermo camera cooling.
13	Thermo camera steady state.
14	Aircraft detection camera operating.
15	All cameras operating, tracking object across sky.
16	Clapping in dome.
17	Tool drop in dome.
18	Walking around in dome.
19	Jumping in dome.
20	Shouting in dome.

5.5 Thermal Experiment on Coude Mirrors

Four temperature sensors were attached to Coude mirrors 4 and 5, the placement of the sensors on the mirror and mounts is shown in figure 8. Also, the locations of Coude mirrors 4 and 5, with respect to the telescope structure, are shown in 9.

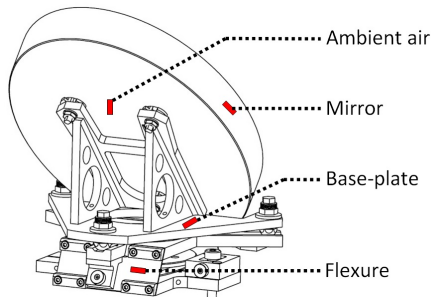


Figure 8: Locations of sensors attached to Coude mirrors 4 and 5. General purpose probe measuring ambient air temperature (suspended behind mirror, not attached to surface), surface mounted probe measuring mirror surface temperature, RTD measuring mirror mount base-plate surface temperature, RTD measuring mirror mount rear flexure surface temperature.

The general purpose probe was suspended between the mirror angle brackets to measure ambient air temperature. Two ceramic Resistance Thermometer Detectors (RTDs) were placed on the mount base-plate and horizontal flexure to measure the surface temperature of the mount. One

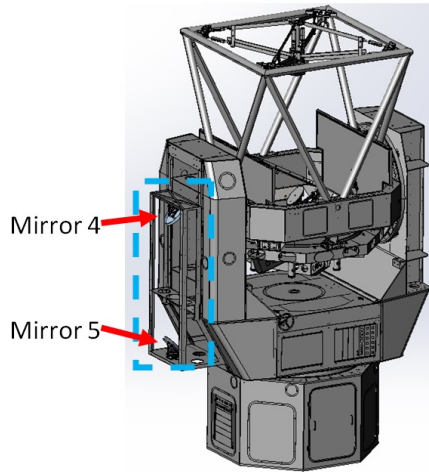


Figure 9: Location of Coude mirrors 4 & 5 in relation to other telescope components.

attachable surface mounted probe was placed on the vertical long-side of the Coude mirror itself. The particular sensors, their location, the data channel that they are attached to, and what they are measuring is shown in Table 8.

Table 8: Columns correspond to mirror 4 or 5, channel number, sensor type, location of sensor, and the particular temperature that that sensor is measuring.

Mirror	Channel	Sensor	Location	Measuring
5	0	Surface mount detector	Side of mirror	Surface temperature
5	1	General purpose probe	Behind mirror	Ambient
5	2	RTD	Mount base-plate	Surface temperature
5	3	RTD	Mount horizontal flexure	Surface temperature
4	4	Surface mount detector	Side of mirror	Surface temperature
4	5	General purpose probe	Behind mirror	Ambient
4	6	RTD	Mount horizontal flexure	Surface temperature
4	7	RTD	Mount base-plate	Surface temperature

The sensor placement is the same for both mirrors. All data-cabling was strain relieved using Kapton tape, cable ties, and M6 and M8 bolts. The data acquisition unit was set to log a temperature reading every second from 11:43 am Friday 12th December 2014 and was stopped at 11:23 Tuesday 6th January 2015. Measuring the temperature every second was to allow determination of the time difference in temperature changes between components of the mounts which could occur at a fast rate. In addition to this sensor data, EOS provided ambient temperature data recorded outside of the dome. This data will allow comparison of how the surface temperatures of the mirrors and their mounts track the ambient outside air temperature.

6 Results and Discussion

6.1 Laser Unit Vibrations

The vibrational spectra of the optical bench where the GSL is being constructed identified small peaks (all approximately 1×10^{-4} ms $^{-2}$) at 48, 75, 100, 238 and 619 Hz. There were also peaks at 314 and 405 Hz small enough to be considered just noise but their appearance in subsequent tests confirms that they are real peaks. How these peaks changed for various different tests is summarised in Table 9.

Table 9: Summary of tests performed on the laser optical bench and the resulting vibrational response with respect to the baseline spectrum.

Description	Response
Chiller ‘a’ running.	Peaks every 50 Hz from 0 to 2100 Hz (max range). This was not altered when vibrations from the chiller were mechanically damped or when the hoses attaching it to the laser were removed.
Chiller ‘b’ running.	Increase in magnitude of 48 and 100 Hz peaks by a factor of 3.5 and 5.4 to 3.5×10^{-4} and 5.4×10^{-4} ms $^{-2}$, respectively. Small increase in all other peaks.
Chiller ‘c’ running.	Increase in 48 and 100 Hz peaks by a factor of 6 and 2 to 6.46×10^{-4} and 1.55×10^{-4} ms $^{-2}$, respectively. New peaks at 184 and 369 Hz were identified with respective magnitudes 2.47×10^{-4} and 1.86×10^{-4} ms $^{-2}$.

Chiller ‘b’ is by far the least disruptive causing only a small increase in the magnitude of peaks already present in the baseline spectrum when nothing is running. Chiller ‘a’ is worse causing a larger increase in peak magnitude and creating vibration at new frequencies. The strange behaviour of chiller ‘c’ is most likely to be an electrical effect. The 50 Hz mains frequency and resulting harmonics could be generated in any electrical component to do with powering the chiller or the chiller itself. As this electrical system extends beyond the chiller itself it could explain why mechanically dampening and isolating the chiller unit had no effect on the resulting vibrational spectra.

The clap tests showed a large magnitude of vibration, 0.1 m s $^{-2}$ peak to peak. This magnitude is on par with a small tap on the table itself. However, the frequency spectrum of claps are dominated by frequencies above 500 Hz. This is not a large problem as the mechanical design of the optical cavities is such that they do not see higher frequencies. Also acoustic vibrations are relatively cheap and easy to damp (rather than redesigning of the laser or laser components) by enclosing the laser unit within acoustic dampening tiles. Tests were also performed confirming that conversational talking, walking softly or door shutting do not cause enough vibrations to deteriorate laser performance.

The most sensitive components of the laser are optical cavities which are constructed of mirrors separated by distances accurate to a fraction of the laser wavelength (in this case a fraction of a micron). The length of these cavities is actively corrected with piezo-actuators connected to a PID controller. The amount of light escaping from these cavities is an indication of laser deterioration and was measured against taps of increasing magnitude. Figure 10 shows the data from two representative tests. The tests with the laser operational and the PID controllers locked onto the light beam show that a disturbance of 0.025 m s $^{-2}$ totaled over all frequencies will cause light to escape the cavity and hence deteriorate the operation of the laser. The magnitude of the tap which caused the PID controllers to lose lock on the light beam and hence cease laser operation in figure

10 TOP was 0.25 m s^{-2} . Spectra of the tap which caused the laser to fail in the top test, a tap that didn't cause the laser to fail and the series of taps in the bottom test are shown in figure 11. The 100 Hz peak is present and equal in magnitude in both the tap that did and didn't stop the laser from working, suggesting that it is not a contributor to laser failure. The rest of the spectrum however was lower with the whole range and the broad peak between 50 and 60 Hz in the no failure tab being about half that of the tap which caused failure. While the tap which caused failure of the first test was larger, the spectra for the first and second tests show similar peaks and magnitudes. The similarity of these spectra indicate that multiple small disturbances can be just as problematic as a single big disturbance. The different responses to single or repeating disturbances could have serious implications in the operation of the laser in the dome as both will be present. This relationship is worth further investigation.

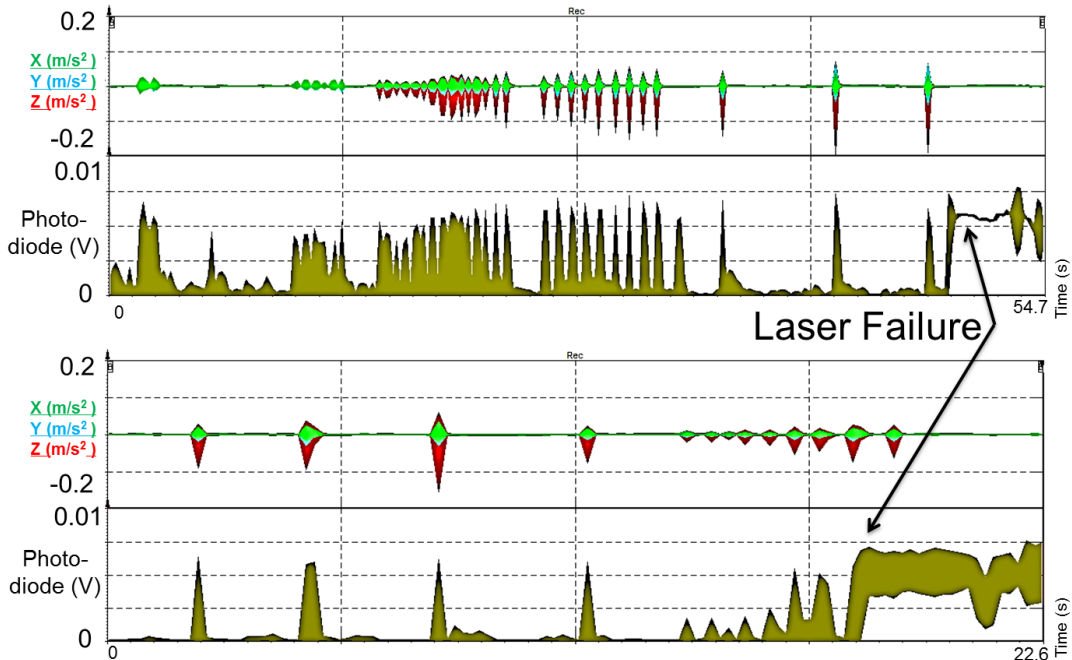


Figure 10: The both top and bottom are separate tests with laser deterioration in brown time correlated against disturbances shown in green, blue and red which correspond to the x , y and z axis, respectively.

Escaping light from optical cavities is a good measure of degradation of the laser in its current state, however the gain settings on the PID controllers which compensate for vibrations have not been finalised. The current operational state of the laser is set to be improved once the ideal gain settings are found. The change in the PID controller will affect the magnitudes at which deterioration and failure occur in the final laser design, but the above analysis of single and repeated disturbances is still valid. The values that have been measured on the current state of the laser for deterioration are still useful to compare to the current conditions in the telescope to provide a measure of how much improvement is necessary.

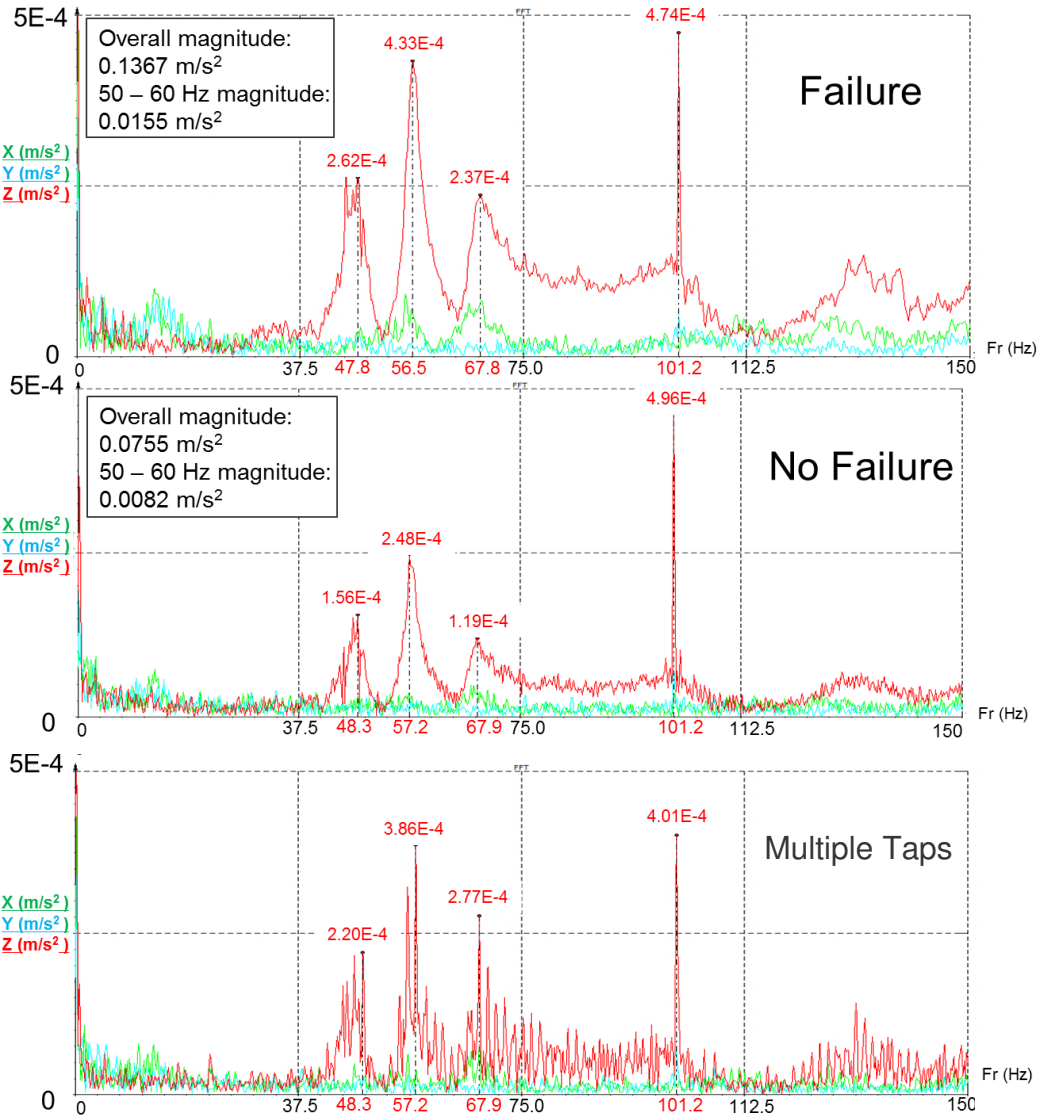


Figure 11: TOP: Spectrum of a single large tap which caused laser failure. BOTTOM: Spectrum of a series of small taps which caused laser failure.

6.2 Telescope Dome

6.2.1 Mechanical Operations

The overall baseline vibrations of the telescope (total acceleration over all frequencies) with no instruments or telescope motion have a magnitude of 0.2 m s^{-2} which is an order of magnitude greater than what it currently takes to deteriorate laser function. The frequency spectrum of this baseline is shown in figure 12. The main peaks of interest in the low frequency band are at 42, 56, 78 and 100. The magnitudes of each of these peaks and any additional peaks that appear in each

mechanical test are summarised in Table 10.

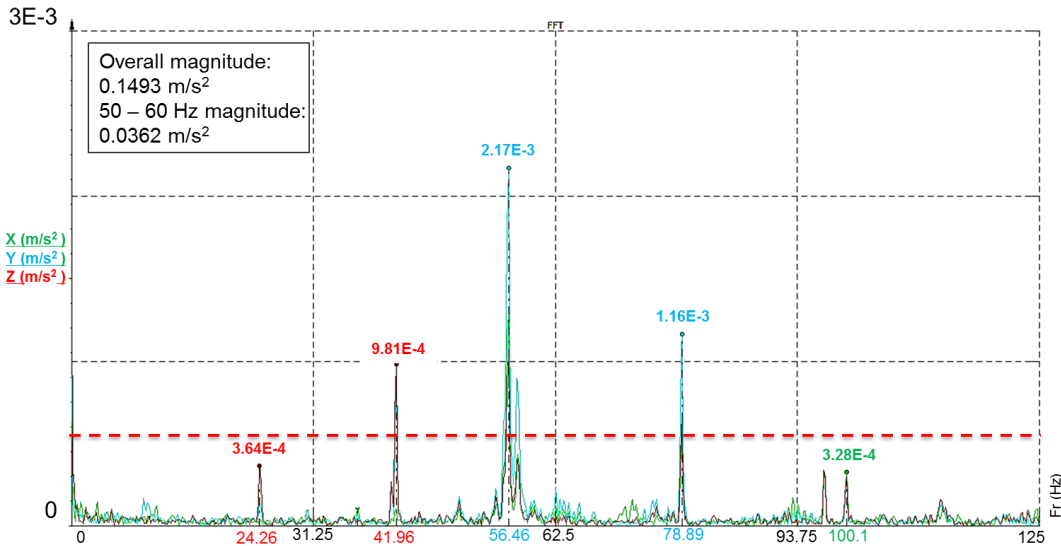


Figure 12: Spectrum of the vibrations present when all systems (telescope, instruments, dome) are at rest.

Table 10: Summary of tests performed in the telescope dome.

Operation	Peak magnitude (mm s^{-2})				Additional peaks (Hz: mm s^{-2})
	42 Hz	56 Hz	78 Hz	100 Hz	
No activity.	0.98	2.17	1.1	3.3	24:0.36
Altitude motion.	3.45	3.83	18.9	1.3	37: 7.85, 84:5.6
Full azimuth rotation.	2.9	11.9	-	13.0	4:17.9, 19:10.1
Tapping left side of GSL mount.	1.7	7.14	5.68	-	
Tapping right side of GSL mount.	1.54	2.45	1.75	0.96	
Tapping trunnion nasmyth.	1.28	2.12	0.937	0.903	
Tapping truss mid head-ring.	1.2	4.6	3.96	1.6	70:5.72 84:3.98
Mirror covers opening.	1.05	2.64	1.28	0.47	24:0.39
Tracking object, all cameras.	4.5	10.5	-	6.0	4:20.9 8:14.6 16:7.08
Walking around dome.	1.21	1.35	1.25	0.86	-

Of the four main frequency peaks identified in the dome two of them are common with the peaks found in the optics lab which caused the laser to stop working, namely 56 and 100 Hz. The 42 Hz peak is also very close to the 48 Hz peak found on the laser. Primary focus should be given to dampening the frequencies that are in common between the two tests as these are frequencies are present in tests which degraded laser functionality. The vibrations of the telescope baseline were larger than the vibrations that caused the laser to fail both over the whole 0 - 150 Hz range and the 50 - 60 Hz broad peak.

One of the most common frequency peaks in the dome was 78 Hz which does not appear as a strong individual peak on the spectrum of the laser environment. Further testing to determine the

effects of a 78 Hz peak vibration on the laser are recommended. If the laser is not degraded by 78 Hz vibrations then one of the largest vibrational components of the dome will not be a problem.

An 84 Hz peak is seen in only two of the tests, the altitude motion and tapping on the mid head-ring. Both of these tests have vibrations being generated near the secondary mirror via tapping or motion of the telescope. If the 84 Hz peaks were an issue the exact cause of them could potentially be identified and improved by careful tightening and placement of counterweights around the mid head-ring. There is currently a counterweight secured by only metal wire to the mid head-ring which would act as a pendulum when excited.

The tracking test with all of the instruments on was done as a worst case scenario test with the telescope moving in both the altitude and azimuth directions constantly. In this case the biggest peaks occurred at very low frequencies which were not present in any of the other tests: 4, 8 and 16 Hz (figure 13). The telescope, being a large structure, will have low resonant frequencies. The tracking test has the telescope constantly accelerating and decelerating which excited these frequencies where the other tests, which had the dome move at constant velocities, failed to. While tracking the vibrations over 150 Hz and the 50 - 60 Hz band are over an order of magnitude greater than what the laser can handle in its current state.

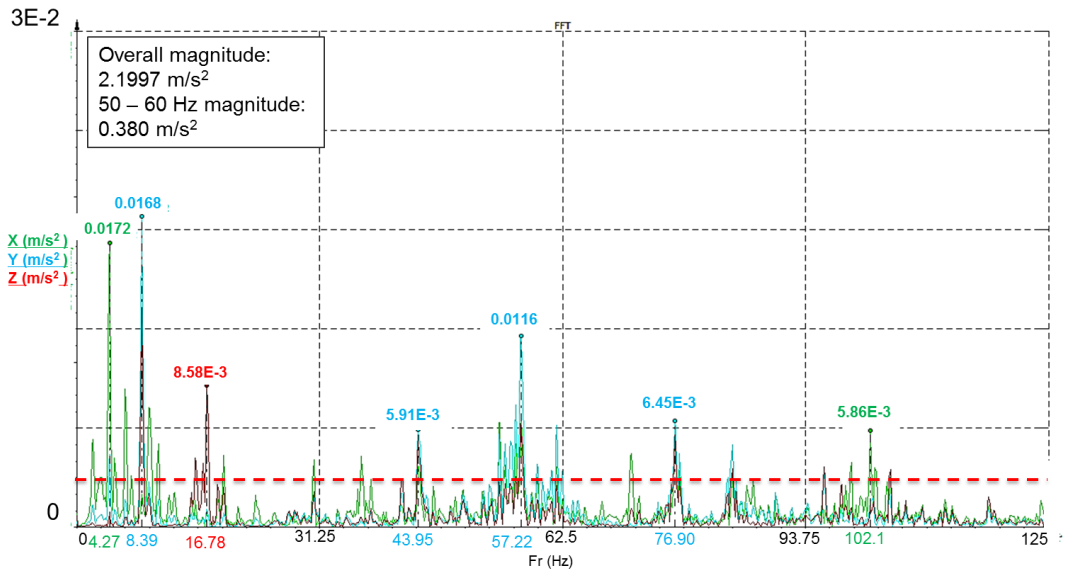


Figure 13: Frequency spectrum of vibrations from the telescope tracking a fast moving target across the sky.

The overall magnitude of vibration, across all frequencies, was always greater in the x -direction. The x direction is the axis perpendicular to the elevation axis, and coplanar with the primary mirror tangential plane. The increased magnitude of vibrations is of importance as it means there will be more movement in the x direction than y or z . When looking at the low frequencies, the peaks in all three directions are even, for instance in figures 12. The extra vibration in the x direction comes from the higher frequencies which are not as much of a concern due to the mechanical design of the laser discussed previously. As the laser bench will be mounted parallel to the xz plane any components that are sensitive to high frequency vibrations should be mounted such that they do not align with the x -direction.

There is a large difference in magnitudes of the peaks between tapping on the right and left side of the GSL mount. This is due to the accelerometer being mounted on the left hand side, resulting in bigger magnitudes detected there, rather than being an indication of asymmetry in the telescope at that location.

6.2.2 Instrumentation

The three instruments tested on the dome were a mid field camera, a thermal camera and an aircraft detection camera. The aircraft detection camera is by far the most disruptive of the three with a very large frequency peak at 78 Hz. This peak is on a magnitude comparable to moving the dome. Of the mid field and thermal cameras the worst case is when they are running their cooling systems at startup. In all cases the spikes are again at 42, 56, 78 and 100 Hz. The numerical values for all of the tests are given below in Table 11. Once the cooling has finished on the thermal camera it was no longer making any vibrations noticeable above the baseline level. This suggests that it would be beneficial for standard procedure to have cameras turned on and cooled, if they are to be used, before the laser is activated.

Table 11: Summary of tests performed in the telescope dome.

Operation	Peak magnitude ($\text{m s}^{-2} \times 10^{-3}$)			
	42 Hz	56 Hz	78 Hz	100 Hz
Aircraft detection.	1.07	1.58	11.8	0.643
Thermal cooling.	1.27	3.7	1.24	0.69
Thermal steady state.	1.24	1.55	1.32	0.913
Mid field cooling.	1.02	3.37	1.19	0.599

6.2.3 Acoustic Vibration

The peaks and magnitudes of both talking and shouting in the dome did not differ significantly from that of the baseline, meaning there is no risk to the laser from conversation above that of the dome environment. The clap and tool drop tests produced acoustic vibrations only. These tests had the largest magnitude of vibration but most of the power was in the higher frequencies (> 200 Hz). A jump on the dome did not have peaks any different from the baseline in the low frequencies which confirms that the dome floor is isolated from the telescope, as it is supposed to be. As before in all of these cases the vibrations in the x direction have been far larger than in the other directions with the higher frequencies being all in the x direction and the low frequencies an even mix of all three axis.

6.3 Thermal Measurements

6.3.1 Maximum and Minimum Temperature Components

Discussed herein are the maximum and minimum temperatures of the inside and outside ambient air, and the surfaces of the Coude mirrors and their mounts. All plots begin at 12:00 midday at zero. The temperature of all mirror elements, as well as the external air temperature, is plotted for the seventeen day block including the external ambient air temperature in figure 14.

It can be seen that all mirror 5 elements are at a higher temperature than the surrounding ambient air. Conversely, it appears that all mirror 4 elements are at a lower temperature than the surrounding ambient air.

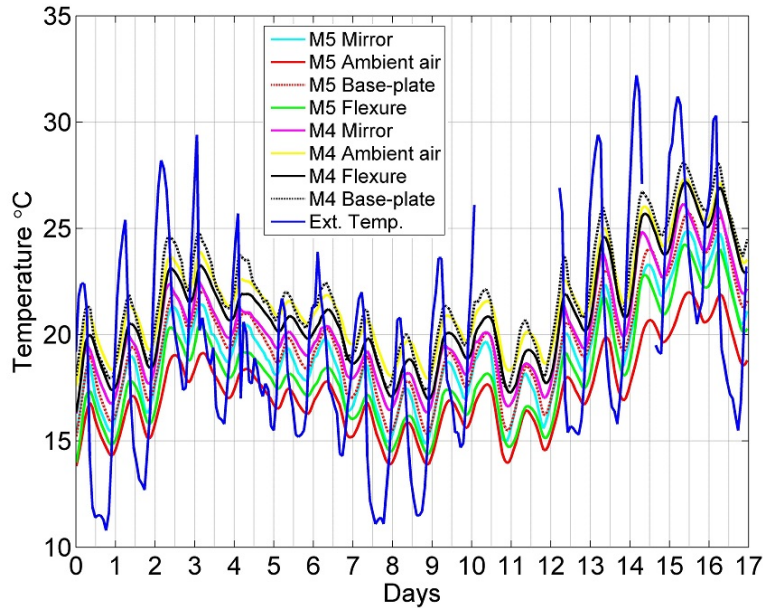


Figure 14: Temperature vs time for all mirror 4 & 5 components as well as external air. Note that the external temperature data-set has two gaps. One starting and finishing at approximately lunchtime of the tenth day and two p.m. of the twelfth day, respectively. The other gap started and finished at approximately 09:00 and 15:00 on the fourteenth day, respectively.

The maximum and minimum temperatures and the difference for each component as well as the internal air temperature surrounding the Coude mirrors were found, Table 12.

Table 12: These are the maximum and minimum temperatures for each component. Also shown is the maximum change in temperature over one day experienced by each component.

Channel	Mirror	Reading	Max (°C)	Min (°C)	ΔT (°C)
0	5	Mirror	24.92	14.83	4.80
1	5	Ambient	22.02	13.73	3.77
2	5	Baseplate	25.74	15.08	4.68
3	5	Flexure	24.26	13.87	4.12
4	4	Mirror	26.19	16.07	4.21
5	4	Ambient	27.38	17.46	3.97
6	4	Flexure	27.20	16.24	4.44
7	4	Baseplate	28.18	17.26	5.03

The maximum change in temperature was experienced by the mirror 4 mount base-plate. The minimum change in temperature was experienced by the ambient air surrounding mirror 5. The mirror 4 mount base-plate is the highest temperature component. The lowest measured temperature was that of the mirror 5 ambient air. It is interesting to note that the change in temperature of the mirrors are relatively close, approximately 0.6 °C. This relatively close change in temperature

is observed for all pairs of components, and is not surprising: the component pairs are essentially duplicates. The average difference in temperature between mirror 4 and mirror 5 was found to be approximately 2.2°C . The difference in height between mirror 4 and mirror 5 is approximately 1.9 m: the temperature difference seems high when only taking this difference in height into consideration. The steel grated floor of the dome may be acting as a thermal barrier, possibly explaining the difference in temperature. Another possible explanation: it was noticed when setting up the sensors around mirror 5 that there was air flowing over the mirror and its components. This mirror may be benefiting from a convective cooling effect.

6.3.2 Lag Times

A three-day time-slice has been selected as a representative sample of results in figure 15.

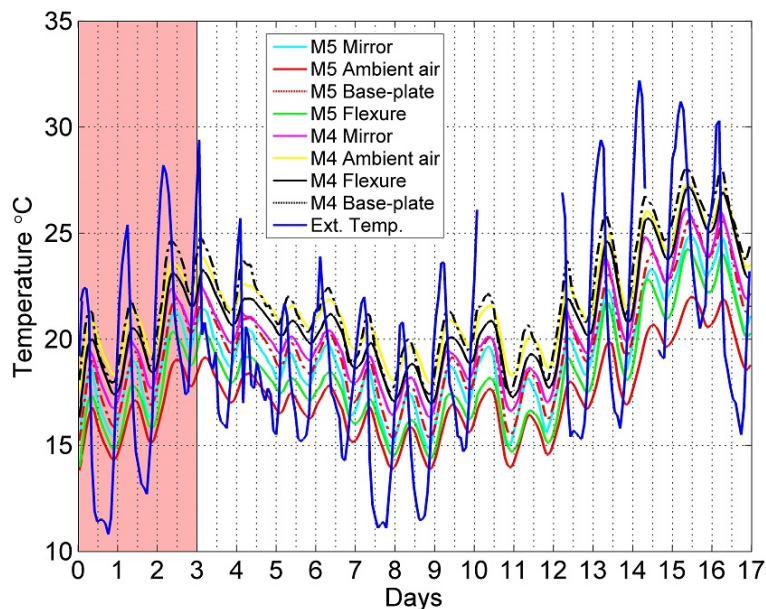


Figure 15: The decay curves fitted using the 3-day data set.

The data represented in the pink rectangle is examined in figure 16.

Maximum external temperature is reached around approximately 14:00-15:00. Maximum internal component temperature is reached around approximately 21:00-22:00. During the day the outside ambient air temperature is acting as a heat reservoir, and the internal components are sinking this heat. The difference between the times of maximum attained temperatures is referred to as lag time. The lag time is due to the rate of heat transfer through the dome, it takes time for the heat to transfer from the outside to the inside. This is due to factors such as: material thermal conductivity; material geometry; convective, conductive and radiative heat transfer. The lag time between the external ambient air temperature and the temperature of the air surrounding mirrors 4 and 5 are 3.9 ± 1.6 and 5.3 ± 1.8 hours, respectively. The height difference between mirrors 4 and 5 may be a factor in this difference in lag time. Again, the possibilities that the steel floor acting as a thermal boundary and mirror 5 convective airflow are considered. It can be seen in figure

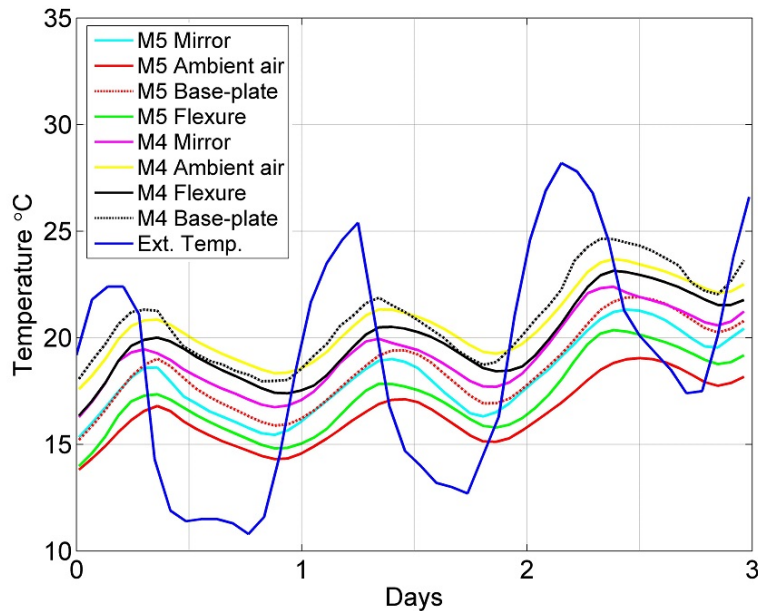


Figure 16: The plot shows the data represented in the pink rectangle above in Figure 15. Note that all curve colours are kept the same for clarity. Note that at all times the ambient air mirror 5 is the lowest temperature component. Conversely, the mirror 4 mount base-plate and ambient air are the hottest components at different times.

17 that the external temperature, as expected, leads the internal mirror and mount component temperatures.

The mirror 4 ambient air heats up quicker than the mirror 5 ambient air. Again this is due to the difference in height and perhaps the grated steel floor.

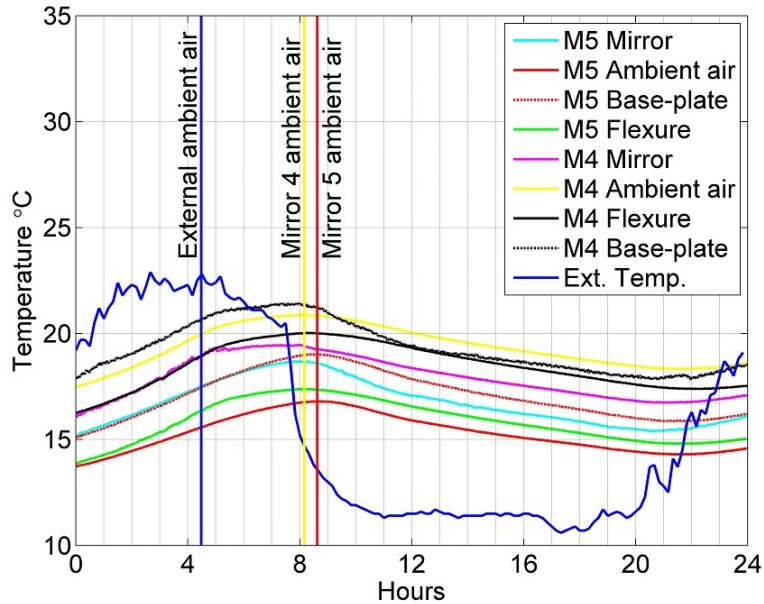


Figure 17: The maximum temperature of the external ambient air and the internal ambient air surrounding both mirrors is marked by a vertical line on the x-axis. The vertical marker lines are the same colour as the curves that they represent.

6.3.3 Decay Curves

The data used to produce the decay curves is shown in figure 18.

Using the data represented in figure 18 the exponential temperature decay rate constants were found for each internal component curve. The fitted decay curves were produced using equation (1)

$$T(t) = T_a + (T_o - T_a)e^{-kt}, \quad (1)$$

where t is the time, $T(t)$ is the component surface temperature as a function of time, T_a is the ambient air temperature at time t , T_o is the initial component surface temperature at $t = 0$ and k is the decay rate constant. The decay curves of the 3-day data set were isolated and the time at which each started and ended was noted. The initial component surface and the ambient air temperatures are known. A script was used to iterate through values of the decay rate constant, k , and produced a least squares fit. The curve of best fit plotted against the measured data is shown in figure 19.

The decay rate constants are tabulated, Table 13.

The component with the greatest decay rate constant is the mirror 5 mount flexure at 4.72×10^{-5} . The component with the lowest decay rate constant is the mirror 5 mount base-plate at 1.63×10^{-5} . It can be seen that the 'Day One' and 'Day Two' columns of Table 13 are quite similar to each other, and relatively different to the 'Day Three' column. The 'Day Three' fit was actually the best fit of the three. While it appears that the values of the constants for 'Day One' and 'Day Two' are quite close together, the fits were quite poor.

A component with a greater decay rate constant will transfer its heat at a higher rate than a component with a lower decay rate constant. It may be reasonable to assume that the decay rate

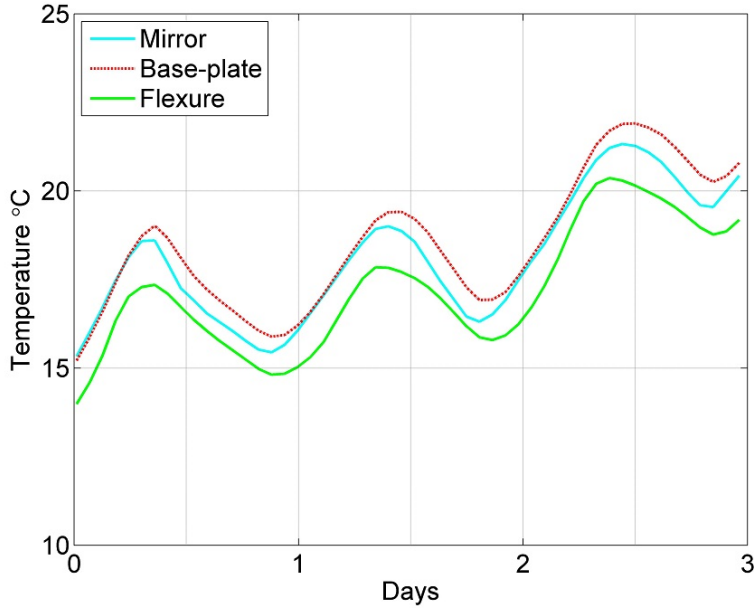


Figure 18: This plot shows temperature vs time data for mirror 5 and its mount flexure and mount base-plate.

Table 13: Maximum and minimum decay rate constants for mirror 5 and its mount base-plate and flexure, k , produced by the curve fitting.

Channel	Day One	Day Two	Day Three
Mirror	4.15×10^{-5}	4.09×10^{-5}	2.46×10^{-5}
Base-plate	2.84×10^{-5}	2.59×10^{-5}	1.63×10^{-5}
Flexure	4.72×10^{-5}	4.20×10^{-5}	2.94×10^{-5}

constant is somewhat dependent upon the thermal conductivity of the material. That is, a material that is less resistant to the transfer of heat will do so more quickly. The experimental data bears this out as the temperature curve of the mirror 5 mount flexure decays at the highest rate. The flexure is made of aluminium which has a thermal conductivity of approximately $205 \frac{W}{mK}$ [28]. The base-plate has a thermal conductivity of approximately $54 \frac{W}{mK}$ [28]. Therefore, it is not surprising that the flexure's temperature curve decays at a higher rate than that of the base-plate. The flexure is able to conduct heat at a greater rate into components that are in contact with and adjacent to it. However, radiative heat transfer effects may also play a role here. The flexure has a shiny appearance whereas the baseplate is a dark brown almost black coloured steel. In other words, aluminium has a lower emissivity than does steel. Consider the equation for radiation heat transfer (2)

$$\dot{Q} = \sigma \varepsilon A (T_H^4 - T_C^4), \quad (2)$$

where σ is the Stefan Boltzmann constant, ε is the material emissivity, A is the area of the

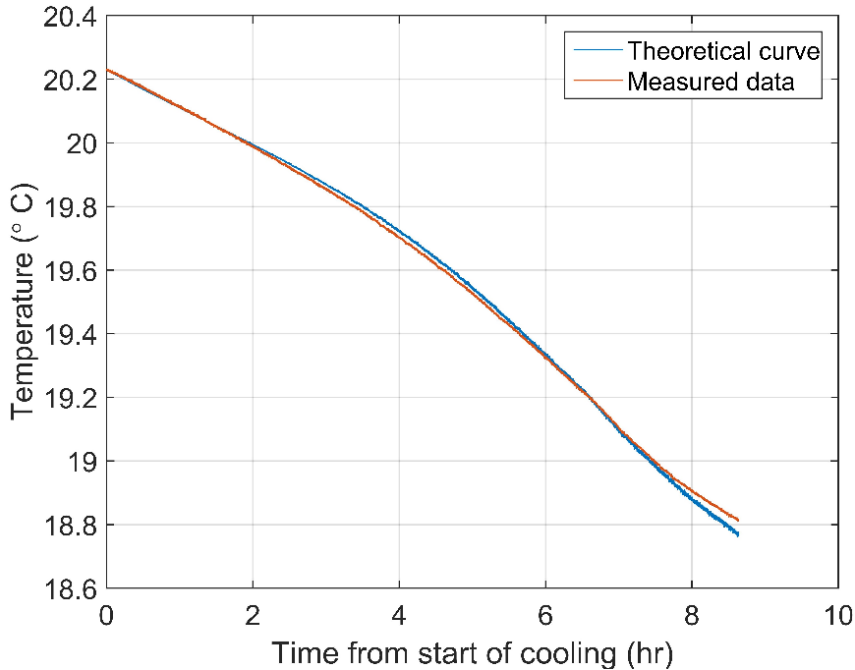


Figure 19: The graph shows the curve of best fit plotted against the measured data from the mirror 5 mount rear flexure. This fit yielded the following values: $k = 2.94 \times 10^{-5}$ and $S = 7.864$. The relatively small value of S suggests that the fit is reasonably accurate.

emitting body, T_H is the absolute temperature of the emitting body, T_C is the absolute temperature of the cooler surroundings. Assuming that all variables are the same, the aluminium flexure will have less heat transferred to it than the steel base-plate - all due to the difference in emissivity. This is illustrated in figure 20. It is reasonable to assume that the flexure, in reality, is able to reflect more of the radiation due to its surface properties. Conversely, the base-plate will most likely absorb more radiation. In this situation heat transfer due to radiation can probably be considered negligible. This is due to the 10^{-8} in the Stefan Boltzmann constant and the relatively low temperatures involved.

7 Conclusions and Recommendations

The measured baseline telescope vibrations are powerful enough to prevent the laser from functioning. Telescope tracking operation vibrations are more powerful than these baseline vibrations. The GSL unit will need to be made more resistant to vibration if it is to function correctly during these routine telescope operations. This resistance is being achieved through fine-tuning of the PID compensators for the optical cavities and the use of more robust and solid optical components in the final product. It is suggested, based on the measured data, that acoustically damping the GSL unit would be a cost efficient method to improve the system. It is also suggested that any components that are directionally sensitive, or sensitive to higher frequencies, are set up such that they are not aligned in the x direction. The maximum magnitude achieved in each of the peak frequencies from the above data are listed together in the Appendix for convenience.

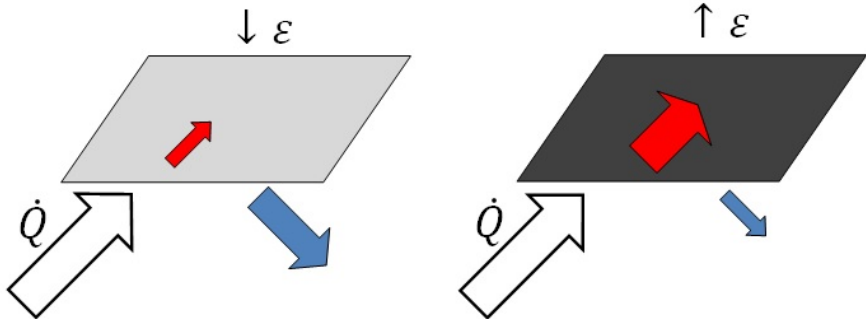


Figure 20: The plates represent aluminium and steel to the right and left, respectively. Heat, represented by \dot{Q} enters each plate. The red arrow shows the proportion of heat absorbed by the material. The blue arrow shows the proportion of heat reflected. ε is the material's emissivity. A greater emissivity corresponds to a greater amount of heat absorption. Aluminium therefore absorbs less heat via radiation than does steel.

Measurements of the surface temperatures of Coude mirrors 4 and 5 yielded maximum and minimum temperature components. These were at 28.2 °C and 22.0 °C for the mirror 4 mount base-plate and the mirror 4 ambient air, respectively. For comparison, the maximum and minimum external ambient air temperature recorded, on the same day, was 32.1 °C and 20.5 °C, respectively. An average temperature difference between mirror 4 and mirror 5 was found to be approximately 2.2 °C. Average lag times between the external ambient air and the internal ambient air temperature were found to be 3.9 and 5.3 hours for mirror 4 and mirror 5, respectively. It is suspected that the steel grated floor that encircles most of the telescope - and separates the upper level from the lower level - is resisting the transfer of heat. This might explain the rather large difference in the lag times. Upon attachment of the mirror 5 temperature sensors it was noted that air was flowing over this mirror. Convective cooling of mirror 5 and its components may account for the relatively large temperature differential. Curve fitting revealed that the mirror 5 mount flexure was the fastest cooling component. It is suggested that this is due to the relatively high thermal conductivity constant of aluminium.

8 Future Work

With respect to further possible testing within the telescope dome it may be of benefit to repeat the tests upon the enclosure that the GSL is to be housed within. One further test that might be performed would be to properly fix - or even temporarily remove - the mid head-ring counterweight and then take measurements to determine whether it is acting as an input. It also may be of interest to perform the optical lab tests again after the PID has been tuned. A relatively large magnitude peak at 78 Hz was detected in the telescope dome. It may be prudent to use an electrodynamic shaker to simulate a 78 Hz input to determine its effect upon the GSL unit. Additionally, further testing should be performed to determine the magnitude and frequency limits at which the laser unit 'loses lock' when subjected to single or multiple quick-succession tap inputs. Finally, it may be interesting to measure the vibration of individual pieces of equipment within the dome to determine the frequency at which they may be providing inputs to the telescope. Equipment to investigate might include: the altitude servo motors, the azimuth motors, the vent shutters when they open or close, the cooling unit, and possibly even the dome walls on a windy day. The temperature sensor

that recorded data on channel 1 should be checked to ensure that it was functioning correctly.

9 Appendix

Table 14: Table of the largest magnitude of vibration at each of the identified frequencies with the causing event.

Frequency (Hz)	Magnitude (mms^{-2})	Causing event
42	4.5	Tracking object, all cameras
56	11.9	Full azimuth rotation
78	11.8	Aircraft detection camera
100	13.0	Full azimuth rotation

References

- [1] John W Hardy. *Adaptive optics for astronomical telescopes*. Oxford University Press, 1998.
- [2] MA Vorontsov and VI Shmalgauzen. The principles of adaptive optics. *Moscow Izdatel Nauka*, 1, 1985.
- [3] Francis Bennet, Rodolphe Conan, Celine D'Orgeville, Murray Dawson, Nicolas Paulin, Ian Price, Francois Rigaut, Ian Ritchie, Craig Smith, and Kristina Uhlendorf. Adaptive optics for laser space debris removal. In *SPIE Astronomical Telescopes+ Instrumentation*, pages 844744–844744. International Society for Optics and Photonics, 2012.
- [4] Francis Bennet, Celine D'Orgeville, Yue Gao, William R Gardhouse, Nicolas Paulin, Ian Price, Francois Rigaut, Ian T Ritchie, Craig H Smith, Kristina Uhlendorf, et al. Adaptive optics for space debris tracking. In *SPIE Astronomical Telescopes+ Instrumentation*, pages 91481F–91481F. International Society for Optics and Photonics, 2014.
- [5] François Roddier. *Adaptive optics in astronomy*. Cambridge university press, 1999.
- [6] Heiner Klinkrad. *Space debris: models and risk analysis*. Springer, 2006.
- [7] Donald J Kessler and Burton G Cour-Palais. Collision frequency of artificial satellites: The creation of a debris belt. *Journal of Geophysical Research: Space Physics (1978–2012)*, 83(A6):2637–2646, 1978.
- [8] Craig Smith, Yue Gao, Jizhang Sang, and Ben Greene. Laser tracking of space debris for precision orbit determination. *Advances in the Astronautical Sciences*, 142, 2011.
- [9] RM Goldstein, SJ Goldstein, and DJ Kessler. Radar observations of space debris. *Planetary and space science*, 46(8):1007–1013, 1998.
- [10] James Mason, Jan Stupl, William Marshall, and Creon Levit. Orbital debris–debris collision avoidance. *Advances in Space Research*, 48(10):1643–1655, 2011.
- [11] J-C Liou and Nicholas L Johnson. Instability of the present leo satellite populations. *Advances in Space Research*, 41(7):1046–1053, 2008.
- [12] Waldemar Bauer, O Romberg, C Wiedemann, G Drolshagen, and P Vörsmann. Development of in-situ space debris detector. *Advances in Space Research*, 54(9):1858–1869, 2014.
- [13] J-C Liou. An active debris removal parametric study for leo environment remediation. *Advances in Space Research*, 47(11):1865–1876, 2011.
- [14] Celine D'Orgeville, Francis Bennet, Mark Blundell, Rod Brister, Amy Chan, Murray Dawson, Yue Gao, Nicolas Paulin, Ian Price, Francois Rigaut, et al. A sodium laser guide star facility for the amu/eos space debris tracking adaptive optics demonstrator. In *SPIE Astronomical Telescopes+ Instrumentation*, pages 91483E–91483E. International Society for Optics and Photonics, 2014.
- [15] Robert Q Fugate, DL Fried, GA Ameer, BR Boeke, SL Browne, PH Roberts, RE Ruane, GA Tyler, and LM Wopat. Measurement of atmospheric wavefront distortion using scattered light from a laser guide-star. 1991.
- [16] M Lloyd-Hart. Taking the twinkle out of starlight, December 2003. URL <http://spectrum.ieee.org/aerospace/astrophysics/taking-the-twinkle-out-of-starlight>.

-
- [17] R Foy and A Labeyrie. Letter to the editor feasibility of adaptive telescope with laser probe. *Astron. Astrophys.*, 152:L29–L31, 1985.
 - [18] RONALDA HUMPHREYS, LEEC BRADLEY, and Jan Herrmann. Sodium-layer synthetic beacons for adaptive optics. *The Lincoln Laboratory Journal*, 5(1):45–66, 1992.
 - [19] D Bonaccini Calia, Yan Feng, Wolfgang Hackenberg, Ronald Holzlöhner, Luke Taylor, and Steffan Lewis. Laser development for sodium laser guide stars at eso. *The Messenger*, 139: 12–19, 2010.
 - [20] Xiong Hu, ZhaoAi Yan, ShangYong Guo, YongQiang Cheng, and JianCun Gong. Sodium fluorescence doppler lidar to measure atmospheric temperature in the mesopause region. *Chinese Science Bulletin*, 56(4-5):417–423, 2011.
 - [21] Singiresu S Rao. *Mechanical Vibrations*. Pearson, 2011.
 - [22] Caroline Kulcsár, Gaetano Sivo, Henri-François Raynaud, Benoît Neichel, Franois Rigaut, Julian Christou, Andres Guesalaga, Carlos Correia, Jean-Pierre Véran, Eric Gendron, et al. Vibrations in ao control: a short analysis of on-sky data around the world. In *SPIE Astronomical Telescopes+ Instrumentation*, pages 84471C–84471C. International Society for Optics and Photonics, 2012.
 - [23] Eric H Anderson, Roger M Glaese, and Douglas Neill. A comparison of vibration damping methods for ground based telescopes. In *SPIE Astronomical Telescopes+ Instrumentation*, pages 70120H–70120H. International Society for Optics and Photonics, 2008.
 - [24] Yann Clenet, Markus E Kasper, Nancy Ageorges, Christopher Lidman, Thierry Fusco, Olivier Marco, Markus Hartung, David Mouillet, Bertrand Koehler, Gerard Rousset, et al. Naco performance: status after 2 years of operation. In *Astronomical Telescopes and Instrumentation*, pages 107–117. International Society for Optics and Photonics, 2004.
 - [25] Andres Guesalaga, Benoit Neichel, Francois Rigaut, James Osborn, and Dani Guzman. Comparison of vibration mitigation controllers for adaptive optics systems. *Applied optics*, 51(19): 4520–4535, 2012.
 - [26] Y Clenet, M Kasper, N Ageorges, C Lidman, T Fusco, OP Marco, M Hartung, D Mouillet, B Koehler, G Rousset, et al. Naos performances: impact of the telescope vibrations and possible origins. In *SF2A-2004: Semaine de l'Astrophysique Francaise*, volume 1, page 179, 2004.
 - [27] Cyril Petit, Jean-Marc Conan, Caroline Kulcsár, Henri-François Raynaud, and Thierry Fusco. First laboratory validation of vibration filtering with lqg control law for adaptive optics. *Optics Express*, 16(1):87–97, 2008.
 - [28] Yunus A Cengel, Robert H Turner, and John M Cimbala. Fundamentals of thermal-fluid sciences. 2008.